EM Analysis of a Conducting Scatterer in Optic Dielectric Waveguide

Chun-Ting Chou and Shyh-Kang Jeng, *Member, IEEE*

***Abstract*— A method to compute the scattered field of curved mirrors and gratings in a dielectric slab waveguide is proposed. In contrast to the beam propagation method (BPM) for this kind of problems, the method of moment is adopted. By introducing the dyadic Green's function in a slab waveguide, the electric field integral equations for induced current distribution on the conducting obstacles are derived. To improve the computational efficiency, the modified Green's function is incorporated into the computation program. With this study, the effects of grooves of gratings and the finite extent of the mirrors in dielectric waveguides can be investigated in more detail.**

***Index Terms*— Gratings, integral equations, slab waveguide, scattering.**

I. Introduction

PERIODIC structures are widely used in integrated-optics field. Through its wavelength selective property, the laser can be operated in single mode, for example, the distributed feedback (DFB) or distributed Bragg reflector (DBR) lasers. For the wavelength division multiplexing (WDM) in optical communication system, the reflection grating can separate lights with different wavelengths from optical fiber as a demultiplexer [1], [2] or a planar spectrometer [3]. It has the advantage of compact size and availability of more channels. Geometric optics is useful for design consideration such as groove pattern and grating constant [4], [5]. A general procedure of BPM to construct gratings with correction of aberration is also presented in [6], but it is restricted to two-dimensional (2-D) device. Besides, the distribution of scattered field cannot be found in these literature. Another approach is the electromagnetic (EM) analysis developed to treat the grating problem as an electromagnetic scattering problem using the Rayleigh expansion with point match method (PPM) or Fourier transform method (FSM). By this method, grooves of grating are restricted not to be too deep or the groove function should be analytic [7]. It also assumes an infinite grooves to apply the Floquet–Bloch theorem, and derives an integral method to obtain a pseudoperiodic scattering field. Furthermore, scattered field of a (2-D) periodic grating with finite number of grooves in dielectric thin-film waveguides is also presented in [8], [9]. However, the effects of the finite extent of the gratings are all neglected in these works. In this study, EM analysis is applied to analyze conducting periodic structures with finite extent in the transverse direction of optical slab waveguide. By evaluating the scattered field, we try to show the effects of groove shapes and finite width of grating structure. With these additional considerations, the reflection gratings can be modified to get better performance at insertion loss and resolution for further researches. Scattered field pattern of arbitrary metal obstacles with various curvature in a slab waveguide will also be investigated.

Manuscript received July 24, 1997; revised February 5, 1998.

The authors are with the Department of Electrical Engineering, National Taiwan University, Taipei, Taiwan 10617 R.O.C.

Publisher Item Identifier S 0733-8724(98)04094-8.

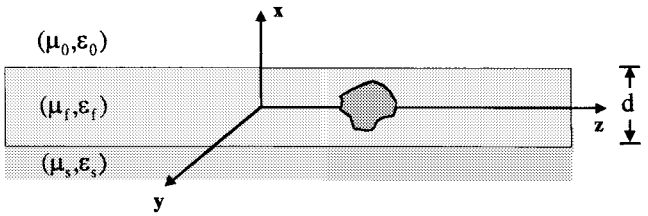

Fig. 1. Cross section of a slab waveguide with conducting scatterer.

It is well known that electric-field integral equations (EFIE) or magnetic-field integral equations (MFIE) can solve scattering from perfect conductors. Since all conducting scatterers are assumed to be thin, the EFIE is better than MFIE [10], and this study adopts the EFIE. For the EFIE, the kernel of the integral equation consists of a dyadic Green's function in a multilayer slab waveguide, which has been derived in spectral domain [11], [12]. Then in this research the obstacle or the grating is divided into N small patches, each has a very small area such that the induced current on each patch can be assumed to be constant. By matching the boundary condition at the centers of all N patches, a linear system of $2N$ equations is obtained. The $2N$ unknowns are the tangential current components of all N patches, each with two components defined in the local coordinate system. With the current distribution, the scattered field can be calculated by the same dyadic Green's function. For far field pattern, simplification can be made to reduce the complexity and increase the computation efficiency without losing the accuracy.

II. Dyadic Green's Function

To obtain the induced current distribution on the conducting scatterer, we should derive the dyadic Green's function in a slab waveguide. Consider a slab waveguide with substrate permittivity ε_s and background permitivity ε_f. As shown in Fig. 1, the x-axis is taken to be perpendicular to the interface, and the z-axis is in the direction of propagation of the incident wave.

In this paper, we restrict the slab waveguide to be symmetric, although the theory can be readily extended to asymmetric

cases. By the image theory, our problem can be divided into an odd part and an even part. The upper half space of the odd part is equivalent to a slab waveguide grounded with a PEC plate, and that of the even part is related to a waveguide with a PMC ground. For our problem, we assume that only the fundamental mode TM_0 is incident, and it will excite only odd modes. Hence, we can consider an equivalent dielectric slab waveguide with a PEC ground only.

Physically, the dyadic Green's function

$$\begin{aligned}\overline{\overline{G}}(\overline{r},\overline{r}') = &\hat{x}\hat{x}G_{xx}(\overline{r},\overline{r}') + \hat{x}\hat{y}G_{xy}(\overline{r},\overline{r}') \\ &+ \hat{x}\hat{z}G_{xz}(\overline{r},\overline{r}') \\ &+ \hat{y}\hat{x}G_{yx}(\overline{r},\overline{r}') + \hat{y}\hat{y}G_{yy}(\overline{r},\overline{r}') \\ &+ \hat{y}\hat{z}G_{yz}(\overline{r},\overline{r}') \\ &+ \hat{z}\hat{x}G_{zx}(\overline{r},\overline{r}') + \hat{z}\hat{y}G_{zy}(\overline{r},\overline{r}') \\ &+ \hat{z}\hat{z}G_{zz}(\overline{r},\overline{r}') \end{aligned} \tag{1}$$

is related to the electric field generated by a point electric current source. For example, $G_{xy}(\overline{r},\overline{r}')$ is the x-component of the electric field at $\overline{r}$ due to a y-directed point source $\delta(\overline{r}-\overline{r}')$ at $\overline{r}'$. Now, let's first consider an x-directed electric current source

$$\overline{J}(\overline{r}) = \hat{x}\delta(\overline{\rho}-\overline{\rho}')\delta(x-x') = \hat{x}J(\overline{r}) \tag{2}$$

where $\overline{\rho} = \hat{y}y + \hat{z}z, \overline{\rho}' = \hat{y}y' + \hat{z}z'$, and $\overline{r} = \hat{x}x + \hat{y}y + \hat{z}z$. Expand

$$J(\overline{r}) = \sum_{n=-\infty}^{\infty} e^{jn\phi}\int_{-\infty}^{\infty}\tilde{J}_n(x,k_\rho)H_n^{(2)}(k_\rho\rho)k_\rho\,dk_\rho \tag{3}$$

where ϕ is the polar angle of $\overline{\rho}-\overline{\rho}'$ measured from the y-axis. From the Appendix, we have

$$\tilde{J}_n(x,k_\rho) = \begin{cases}\dfrac{1}{4\pi}\delta(x-x'), & n=0 \\ 0, & n\neq 0.\end{cases} \tag{4}$$

The magnetic vector potential $\overline{A}$ due to $\tilde{J}(\overline{r})$ satisfies

$$\nabla^2\overline{A} + k_i^2 A = -\mu_o\overline{J} \tag{5}$$

where $k_i^2 = \omega\mu_o\varepsilon_i$, and $i = s$ or f to indicate the region outside or inside the slab. With $\overline{A} = \hat{x}\mu_o\Psi$, we write Ψ as

$$\Psi = \sum_{n=-\infty}^{\infty} e^{jn\phi}\cdot\int_{-\infty}^{\infty}\tilde{\Psi}_n(x,k_\rho)\cdot H_n^{(2)}(k_\rho\rho)\cdot k_\rho\,dk_\rho. \tag{6}$$

By substituting (6) into (5), and keeping only the $n=0$ term by symmetry consideration to achieve

$$\frac{\partial^2\tilde{\Psi}_i(x,k_\rho)}{\partial x^2} + k_{xi}^2\tilde{\Psi}_i(x,k_\rho) = \frac{1}{4\pi}\delta(x-x') \tag{7}$$

where $k_{xi}^2 = k_i^2 - k_\rho^2$. By matching the boundary conditions, the wave function $\tilde{\Psi}_i$ in region i can be obtained for the dielectric slab and the background.

To get the components of $\overline{\overline{G}}(\overline{r},\overline{r}')$ due to the y- or the z-directed sources, we start by considering an arbitrary surface current source parallel to the y-z plane at $x = x'$. From electromagnetic theory [14], the generated field due to such a source can be written as a linear combination of a TM_x field and a TM_x field. For the TM_x part, the field is related to a magnetic vector potential $\overline{A} = \hat{x}\mu_o\Psi$, and Ψ is also in the form of (6). Its components $\tilde{\Psi}_n$ also satisfy (7), except that the right hand side source term is set to be zero. This equation is easily solved first. Then boundary conditions including the source condition at $x = x'$ are applied to get a TM_x solution. For the TE_x part, the field is corresponding to an electric vector potential $\overline{F} = \hat{x}\varepsilon_i\Psi$, and Ψ is again written in the form of (6). The related $\tilde{\Psi}_n$ also satisfies a source-free version of (7). By solving the differential equation, and matching boundary conditions as well as the source condition at $x = x'$, we obtain the TE_x solution.

From the above procedures, we also derive the TM_x current (corresponding to the TM_x field) and the TE_x current (corresponding to the TE_x field) in the form of

$$\begin{aligned}\overline{J} &= \hat{\rho}J_\rho(\rho,\phi) + \hat{\phi}J_\phi(\rho,\phi) \\ &= \sum_{n=-\infty}^{\infty} e^{jn\phi}\int_{-\infty}^{\infty}\left[\hat{\rho}\tilde{J}_{\rho n}(k_\rho) + \hat{\phi}\tilde{J}_{\phi_n}(k_\rho)\right]H_n^{(2)}(k_\rho\rho)k_\rho\,dk_\rho\end{aligned} \tag{8}$$

and

$$\tilde{J}_{\phi n}^{\mathrm{TM}} = \tilde{J}_{\rho m}^{\mathrm{TM}} = \tilde{J}_n^{\mathrm{TM}}(k_\rho) \tag{9}$$

$$\tilde{J}_{\phi n}^{\mathrm{TE}} = -\tilde{J}_{\rho m}^{\mathrm{TE}} = \tilde{J}_n^{\mathrm{TE}}(k_\rho). \tag{10}$$

Hence, for $\overline{J} = \hat{y}\delta(\overline{\rho}-\overline{\rho})$ and $\overline{J} = \hat{z}\delta(\overline{\rho}-\overline{\rho})$ at $x = x'$

$$\tilde{J}_n^{\mathrm{TE}} = \begin{cases}\dfrac{j}{8\pi k_\rho}, & n = 1 \text{ or } -1 \\ 0, & \text{otherwise}\end{cases} \tag{11}$$

$$\tilde{J}_n^{\mathrm{TM}} = \begin{cases}\dfrac{1}{8\pi k_\rho}, & n = 1 \\ \dfrac{-1}{8\pi k_\rho}, & n = -1 \\ 0, & \text{otherwise.}\end{cases} \tag{12}$$

We thus find $\tilde{\Psi}_1^{\mathrm{TE}}$ and $\tilde{\Psi}_1^{\mathrm{TM}}$, and

$$\Psi^{\mathrm{TE}} = 2j\cdot\sin\phi\cdot\int_{-\infty}^{\infty}\tilde{\Psi}_1^{\mathrm{TE}}(x,k_\rho)\cdot H_1^{(2)}(k_\rho\rho)\cdot k_\rho\,dk_\rho \tag{13}$$

$$\Psi^{\mathrm{TM}} = 2\cdot\cos\phi\cdot\int_{-\infty}^{\infty}\tilde{\Psi}_1^{\mathrm{TM}}(x,k_\rho)\cdot H_1^{(2)}(k_\rho\rho)\cdot k_\rho\,dk_\rho. \tag{14}$$

Through (13) and (14), the total field for an arbitrary surface current source at $x = x'$ can be obtained. Using this method we may solve the field due to $\overline{J} = \hat{y}\delta(\overline{\rho}-\overline{\rho}')$and $\overline{J} = \hat{z}\delta(\overline{\rho}-\overline{\rho}')$ at $x = x'$, and the components of the dyadic Green's function are solved.

In practical computation, we apply $H_n^{(2)}(-z) = (-1)^n[H_n^{(2)}(z) - 2J_n(z)]$ to rewrite (13) and (14) as

$$\Psi^{\mathrm{TE}} = -2\sin\phi\int_0^{\infty}\tilde{\Psi}_1^{\mathrm{TE}}(x,k_\rho\rho)k_\rho\,dk_\rho \tag{15}$$

$$\Psi^{\mathrm{TM}} = -2\cos\phi\int_0^{\infty}\tilde{\Psi}_1^{\mathrm{TM}}(x,k_\rho)J_1(k_\rho\rho)k_\rho\,dk_\rho \tag{16}$$

in order to halve the integration interval and avoid the singularity of Hankel function. Note also the property

$$G_{xy}(\overline{r},\overline{r}') = G_{yx}(\overline{r}',\overline{r}), G_{xz}(\overline{r},\overline{r}') = G_{zx}(\overline{r}',\overline{r})$$
$$G_{yz}(\overline{r},\overline{r}') = G_{zy}(\overline{r}',\overline{r})$$

by reciprocity can be used to reduce the derivation work.

III. E-Field Integral Equation for Current Distribution

To find the induced current distribution, consider a current source at point $\overline{r}'$ and the observation point at $\overline{r}$. The current distribution at $\overline{r}'$ is defined by the local right-hand Cartesian coordinate

$$\overline{J} = \hat{x} \cdot J_x' + \hat{t}' \cdot J_t' \tag{17}$$

where t' denotes the tangential unit vector of source plane. The electric field at observation point generated by the current source of a small patch around $\overline{r}'$ is

$$d\overline{E} = \overline{\overline{G}}(\overline{r},\overline{r}') \cdot \overline{J}(\overline{r}') \cdot ds' \tag{18}$$

where $\overline{\overline{G}}(\overline{r},\overline{r}')$ is the dyadic Green's functions whose components have been discussed in last section. Since the surface current contains x-directed and t-directed components, only four field components should be considered; that is $G_{xx}, G_{xt}, G_{t'x}$, and $G_{t't}$ where the first subscript denotes the field component of observation point and the second subscript denotes the current component on source plane. Then, the contribution of current source to the observed field can be obtained from dyadic Green's function derived earlier with some coordinate transforms. By the PEC boundary condition, the tangential field vanished on the scatterer, and the E-field integral equation could be obtained as

$$\hat{n} \times \Big\{ E_{\text{incident},x} \cdot \hat{x} + \sin\theta E_{\text{incident},z} \cdot \hat{t} + \int_{s'} \Big\{ J_x' \Big[G_{xx}\hat{x} + G_{xt}\hat{t} \Big] + J_{t'}' \Big[G_{t'x}\hat{x} + G_{t't}\hat{t} \Big] \Big\} ds' \Big\} = 0$$

The method of moment is then applied to transform the integral equation into a linear system of equations. Rectangular pulse function is used as the basis function such that the current is uniform within the surface and vanish outside it. The Dirac function is chosen to be the weighting function (the point-matching method). A $2N \times 2N$ equation system is derived as

$$\sum_{n=1}^{N} [J_{x_n} \cdot G_{xx} + J_{t_n} \cdot G_{t_n x}] \Delta s' = -E_{\text{incident},x_j} \tag{19}$$

$$\sum_{n=1}^{N} [J_{x_n} \cdot G_{xt_j} + J_{t_n} \cdot G_{t_n t_j}] \Delta s' = -\sin\theta_j \cdot E_{\text{incident},z_j} \tag{20}$$

By solving this matrix equation, we can solve the induced current, and the excited scattered field can be evaluated by summing the contributions from every patches on scatterers.

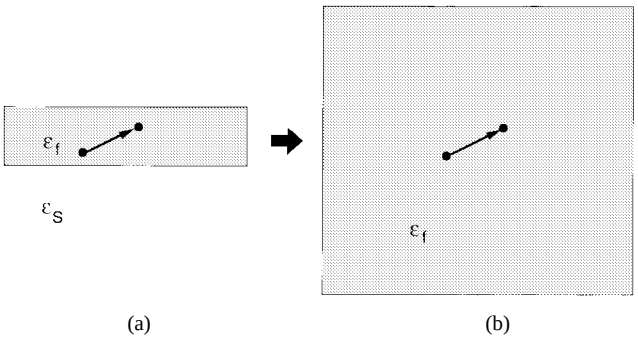

Fig. 2. Approximation for (a) original slab waveguide and (b) infinite space with dielectric constant.

IV. Modified Green's Function

The Green's function, which is an improper integral of k_ρ, will decay as $1/k_\rho$ when the source point and field point are very close. To integrate more efficiently and accurately, the Green's function must be handled separately in such case. To illustrate the modification, we consider the G_{xx} component in Fig. 2(a). When $x \cong x'$ and $k_\rho \gg k_f$, the wave function can be approximated as

$$\Psi_{\text{slab}}(k_\rho) = \frac{1}{8\pi \cdot k_\rho} \cdot e^{-k_\rho |x-x'|}$$

which is identical to that in an infinite space with dielectric constant ε_f [Fig. 2(b)]

$$\Psi_{\text{infinite}}(k_x) = \frac{1}{8\pi \cdot j \cdot k_x} \cdot e^{-jk_x \cdot |x-x'|}$$

if $k_x = -\sqrt{k_f^2 - k_\rho^2}$ is applied. Because the infinite space Green's function has a closed form, the slab waveguide Green's function can be divided into two parts

$$G_{xx} = \int_0^\infty (\Psi_{\text{slab}} - \Psi_{\text{infinite}}) \cdot 2J_0(k_\rho \cdot \rho)\, dk_\rho + \text{Closed-form of infinite space Green's function}$$

where the first part will converge in a smaller integral interval and the integration will be more efficient. All other components of the dyadic Green's function can be treated in the same way. In addition, more cares must be taken for the singular case where the source point and the field point are in the same patch. For regular cases, all fields can be computed by exchanging the order of integration and differentiation to evade the error resulted from the numerical differentiation. But for singular cases, the numerical nine-point differentiation must be adopted after numerical integration.

V. Numerical Results and Discussions

In our numerical simulation, the slab waveguide is designed to support only a single mode, the fundamental odd TM mode. The film layer's refractive index is assumed to be 3.2 and that of the cover layer is 3.0. The effective refractive index for this waveguide is 3.115 and $h = 0.622\lambda_{\text{effective}}$. The problems are divided into three categories: planar obstacles (type I), scatterers with curvatures (type II), and periodic grating structures (type III). Type I scatterers are mainly used

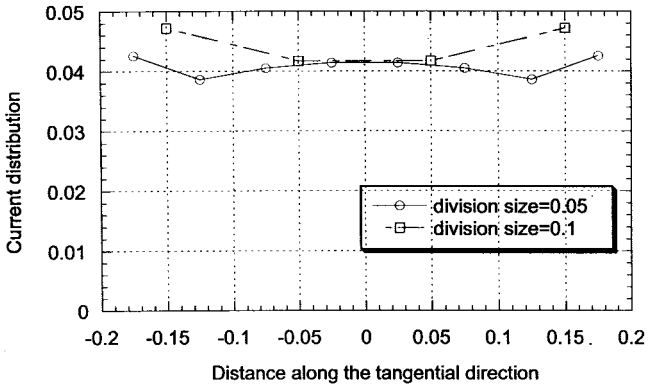

Fig. 3. Convergence with respect to division size.

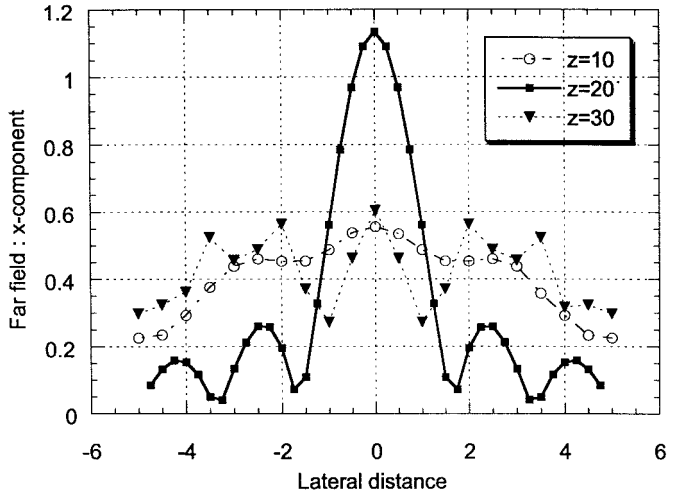

Fig. 4. Scattered field for normal incidence to a curved mirror with focal length = 20 h.

to verify our method. Type II scattterers are designed to observe the focusing effect and type III structures are used to observe the light-splitting phenomena.

First the convergence of the size of subdivision is examined. A PEC plate with size 0.2 h × 0.4 h is normally illuminated. Fig. 3 shows that the current distribution has the maximal error of 10% for patch sizes 0.1 and 0.05 h. Since there is a tradeoff between patch size and numerical accuracy, the patch size is chosen to be 0.1 h for compromise between efficiency and error tolerance. Next, a type II scatterer, a curved mirror with focal length to be 20 h and normal incidence, are investigated. The scattered field is concentrated within ±4.3° of the center of the conducting mirror as shown in Fig. 4. The first sidelobe is just 17 dB below the main beam, which demonstrates the focusing effect of the curved mirror. Fig. 5(a) shows the structure of a curved mirror with a focal length of 25 h and Fig. 5(b) is the computed results for this structure with an oblique incident angle $\theta = 45°$. A main beam is observed far from the center of the curved mirror at a reflection angle about 45° (with respect to the normal direction at the center of the curved mirror), which is consistent with the reflection theorem, as shown in Fig. 5(b).

For type III structure, an oblique incidence case with incident angle $\theta = 30°$ shown in Fig. 6(a) is considered first. Fig. 6(b) shows the scattered field observed at 20 h away from

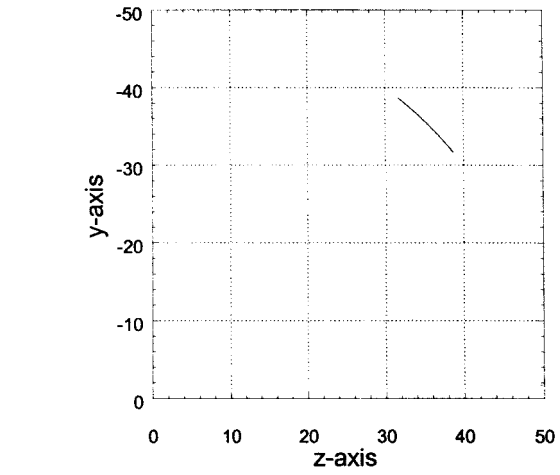

(a)

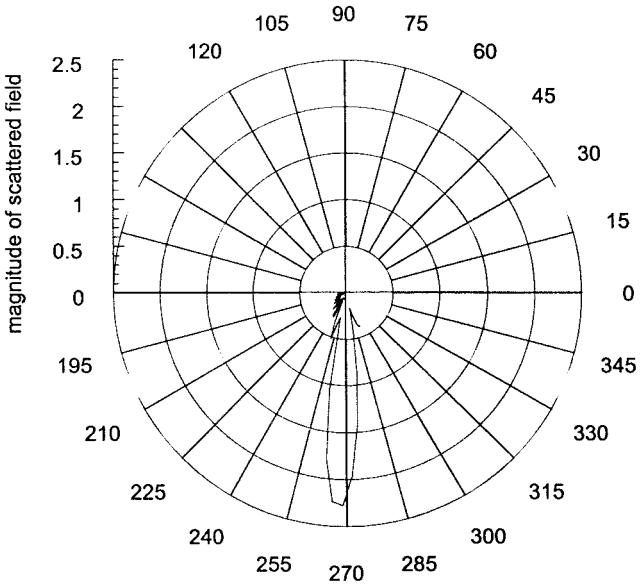

(b)

Fig. 5. Oblique incidence to a curved mirror with incident angle = 45 degrees. (a) Structure of curved mirror. (b) Scattered electric field pattern.

the grating, and two dominant lobes are observed at reflection angle $\theta_R^{(0)} = 27°$ and $\theta_R^{(-1)} = 21°$, respectively (with respect to the normal direction of the grating plane). Since the period of the grating Λ is $1.24\lambda_{\text{eff}}$, according to the grating reflection law [13]

$$\sin\theta_R^{(m)} = \sin\theta_{\text{incid}} + \frac{m\lambda}{\Lambda}$$

there will be a zeroth-order lobe at $\theta = 30°$ and a first-order lobe at $\theta = -17.8°$. The results deviate from the classical theorem significantly since the grating reflection equation [13] is based on the assumption of periodicity of grating, which ignores the effect of finite number of grooves. Thus our results demonstrate how scattering field is affected by the finite extent of grating. The third grating lobe is also observed, which is mainly resulted from the contribution of the top edge of the finite grating. The magnitude ratio of the order one lobe to the order zero lobe is about 1.085, which can be changed by the grating structure. Next we consider a grating the same as the above case but with normal incidence. The number of

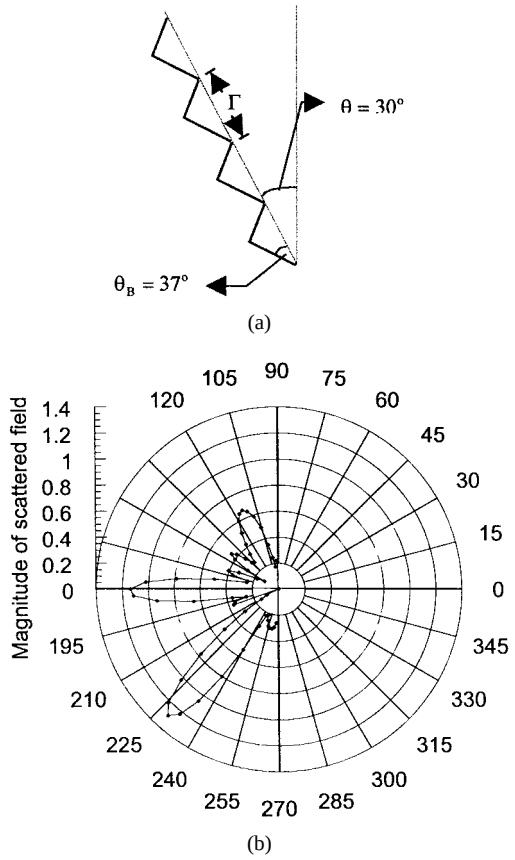

Fig. 6. Oblique incidence to a grating with incident angle = 30°. (a) Structure of grating. (b) Scattered electric field pattern.

the groove has been doubled as shown in Fig. 7(a) and the scattered electric field are observed at 30 h away from the center of the grating as shown in Fig. 7(b). According to the grating law and the 0° incident angle, there will be an order zero, an order one, and an order -1 whose reflection angles are 0, 53.7, and $-53.7°$, respectively. The magnitude ratio of the order 1 to the order -1 is about 1.64, which is obvious since the grating is asymmetric. Compared to the first example of type III scatterers, the diffracted angles, $\pm 54°$, agree with the grating law with error less than 1%. It shows that the classical theorem will predict the scattering field accurately by increase the number of groove. We can also find that the order zero lobe does not focus very well. To improve the resolution, we consider a symmetric grating mounted on a curved surface as shown in Fig. 8(a). The period of the grating is 2.6 h and the focal length of the curved surface is 26 h. The scattered field is observed at the focal circle of the curved grating. According to grating law, there will be order 0, 1, and -1 lobes whose reflection angles are 0, 38.3, and $-38.3°$, respectively, which are consistent with the scattered field pattern shown in Fig. 8(b). Besides, the width of the reflecting beam decreases because we mount the grating on a curved surface. Based on these design considerations, we can improve the resolution of the reflecting grating by changing the groove shape or the curvature of the mounted surface.

VI. Conclusions

In this study, EM analysis has been applied to the scattering problems of three types of conducting scatterers in a slab waveguide. The dyadic Green's functions for current sources have been derived. The modified Green's functions is also obtained to improve the computational efficiency. A number of numerical results have been presented to illustrate the characteristics of conducting scatterers, such as current distributions on the obstacles, focusing-effect and light-splitting phenomena of gratings. Instead of the periodicity assumption in classical theorems, the proposed method can treat scatterers with finite extent.

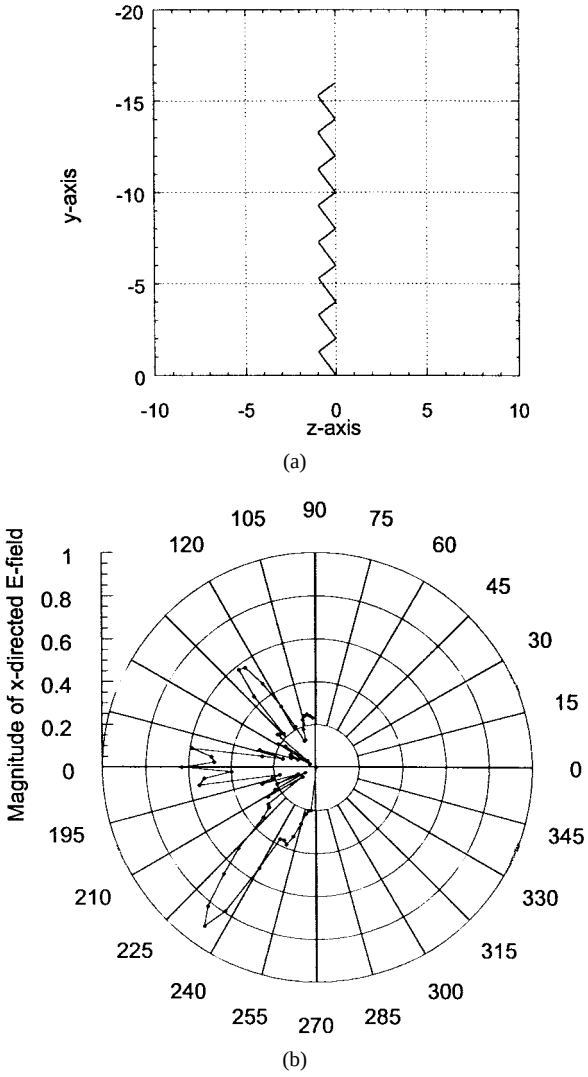

Fig. 7. Normal incidence to a grating. (a) Structure of grating. (b) Scattered electric field pattern.

By suitable modification and extension, the EM analysis can be applied in handling more general scattering problems in a slab waveguide. It is also useful for microwave and millimeter-wave applications.

Appendix

In this Appendix, each mode of dyadic current source is introduced. Consider a delta current source

$$J = \delta(x - x')\delta(y - y')\delta(z - z'). \tag{A.1}$$

By the definition of delta function $\delta(y - y') =$

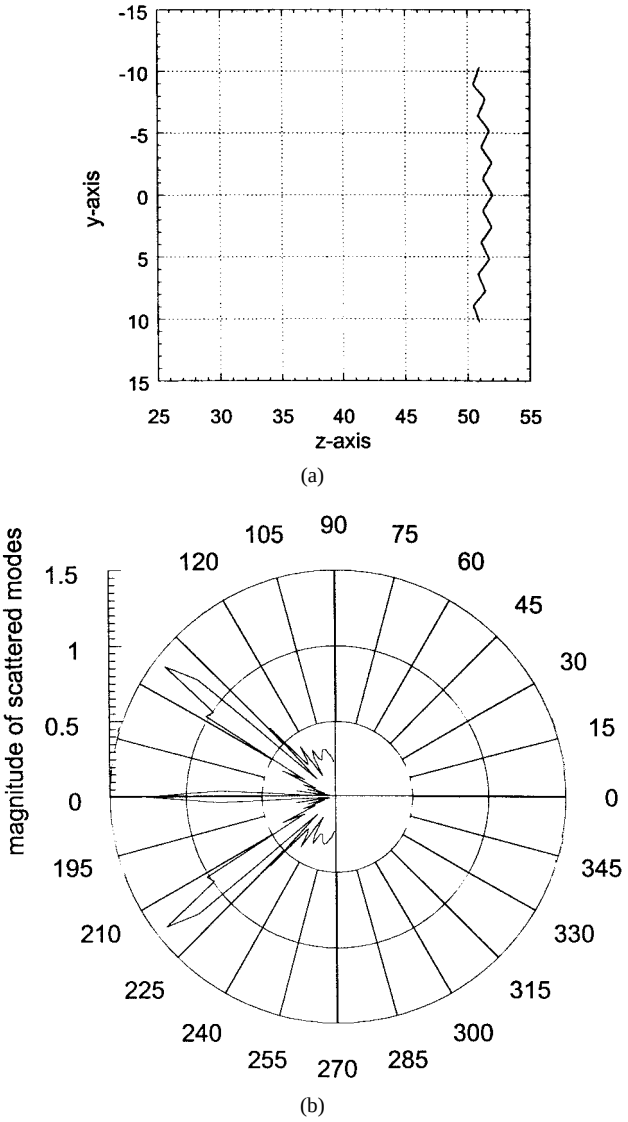

(a)

(b)

Fig. 8. Normal incidence to a grating mounted on a circle with focal length = 26 h. (a) Structure of grating. (b) Scattered electric field pattern.

$(1/2\pi) \int e^{j\cdot k_y\cdot(y-y')}\, dk_y$, then

$$\delta(\overline{\rho}-\overline{\rho}') = \frac{1}{4\pi^2}\int_{-\infty}^{\infty}\int_{-\infty}^{\infty} e^{j[k_y(y-y')+k_z(z-z')]}\, dk_y\, dk_z. \tag{A.2}$$

With the aid of Bessel's equality $(1/2\pi)\int_0^{2\pi} e^{jx\cos(\alpha-\phi)}\, d\alpha = J_0(x)$ and $H_n^{(1)}(e^{j\pi x}\cdot x) = -e^{-jn\pi}H_n^{(2)}(x)$, (A.2) is transformed to a polar form.

$$\delta(\overline{\rho}-\overline{\rho}') = \frac{1}{4\pi}\int_{-\infty}^{\infty} H_0^{(2)}(k_\rho\cdot\rho)\cdot k_\rho\, dk_\rho. \tag{A.3}$$

Substitute (A.3) into (A.1) and compare the coefficient of (A.3) with the expansion form (1), only $n=0$ mode will exist

$$\tilde{J}_n(x,k_\rho) = \begin{cases} \dfrac{1}{4\pi}\delta(x-x'), & n=0 \\ 0, & n\neq 0 \end{cases}$$

For y-directed and z-directed delta currents, the components of TM_x current and TE_x current can be derived by the following relations:

$$\tilde{J}_n^{\mathrm{TE}} = \frac{1}{2k_\rho}[j\cdot(\tilde{J}_{y,n-1}+\tilde{J}_{y,n+1}) + (\tilde{J}_{z,n-1}-\tilde{J}_{z,n+1})] \tag{A.4a}$$

$$\tilde{J}_n^{\mathrm{TM}} = \frac{1}{2k_\rho}[j\cdot(\tilde{J}_{u,n-1}-\tilde{J}_{y,n+1}) + (\tilde{J}_{z,n-1}+\tilde{J}_{z,n+1})] \tag{A.4b}$$

where $\tilde{J}_{yn}$ or $\tilde{J}_{zn}$ are derived in (A.3).

REFERENCES

[1] P. C. Clemens, R. Marz, A. Reichelt, and H. W. Schneider, "Flat-field spectrograph in SiO_2/Si," *IEEE Photon. Technol. Lett.*, vol. 4, pp. 886–887, 1992.

[2] P. C. Clemens, G. Heise, R. Marz, H. Michel, A. Reichelt, and H. W. Schneider, "8-channel optical demultiplexer realized as SiO_2/Si flat-field spectrograph," *IEEE Photon. Technol. Lett.*, vol. 6, pp. 1109–1111, 1994.

[3] J. B. D. Soole and A. Scherer *et al.*, "Monolithic InP-based garting spectrometer for wavelength-division multiplexed system at 1.5 μm," *Electron. Lett.*, vol. 27, pp. 132–134, 1991.

[4] H. Noda T. Namioka, and M. Seya, "Geometric theory of the grating," *J. Optic. Soc. Amer.*, vol. 64, pp. 1031–1036, 1974.

[5] K. A. McGreer, "A flat-field broadband spectrograph design," *IEEE Photon. Technol. Lett.*, vol. 7, pp. 397–399, 1995.

[6] R. Marz and C. Cremer, "On the theory of planar spectrographs," *J. Lightwave Technol.*, vol. 10, pp. 2017–2022, 1992.

[7] R. Petit, Ed., *Electromagnetic Theory of Grating*. New York: Springer, 1980, pp. 6–26 and pp. 63–74.

[8] A. S. Andrenko and A. I. Nosich, "H-scattering of thin-film modes from periodic gratings of finite extent," *Microwave Optic. Technol. Lett.*, vol. 5, pp. 333–337, 1992.

[9] A. I. Nosich and A. S. Andrenko, "Scattering and mode conversion by a screen-like inhomogeneity inside a dielectric slab waveguide," *IEEE Trans. Microwave Theory Tech.*, vol. 42, pp. 298–307, 1994.

[10] D. L. Knepp and J. Goldhirsh, "Numerical analysis of electromagnetic radiation properties of smooth conducting bodies of arbitrary shape," *IEEE Trans. Antennas Propagat.*, vol. 20, pp. 383–385, 1972.

[11] N. K. Das and D. M. Pozar, "A generalized spectral-domain Green's function for multilayer dielectric substrate with application to multilayer transmission lines," *IEEE Trans. Microwave Theory Tech.*, vol. 35, pp. 326–335, 1987.

[12] H. J. M. Bastiaansen, N. H. G. Baken, and H. Blok, "Domain integral analysis of channel waveguides in anisotropic multi-layered media," *IEEE Trans. Microwave Theory Tech.*, vol. 40, pp. 1918–1926, 1992.

[13] H. A. Haus, *Waves and Fields in Optoelectronics*. Englewood Cliffs, NJ: Prentice-Hall, 1984, pp. 46–49.

[14] R. F. Harrinton, *Time-Harmonic Electromagnetic Fields*. New York: IEEE Press, 1993.

Chun-Ting Chou was born in Taipei, Taiwan, China, on January 26, 1973. He received the B.S. and M.S. degrees in electrical engineering from the National Taiwan University, Taipei, Taiwan. in 1995 and 1997, respectively.

His topics of interest include fiber optics, optical communication, planar mulitplexer, and numerical techniques in electromagnetics.

Shyh-Kang Jeng (M'87) was born in I-Lan, Taiwan, China, on May 6, 1957. He received the B.S.E.E. and Ph.D. degrees from the National Taiwan University, Taipei, Taiwan, China, in 1979 and 1983, respectively.

In 1981, he joined the faculty of the Department of Electrical Engineering, National Taiwan University, Taipei, where he is now a Professor. From 1984 to 1985 he was an Electronic Data Processing Officer and an Instructor of Information System Analysis and Design at National Defense Management College, Chung-Ho, Taiwan. From 1985 to 1993, he was a Visiting Research Associate Professor and a Visiting Research Professor at the University of Illinois, Urbana-Champaign, several times. His current research interest is in electromagnetic scattering analysis and visualization, 3-D sound, music system, and indoor and outdoor channel modeling for wireless communications.